Dependence of Generation of Whistler Mode Chorus Emissions on the Temperature Anisotropy and Density of Energetic Electrons in the Earth's Inner Magnetosphere

Katoh, Y.
Omura, Y.
Miyake, Y.
Usui, H.
Nakashima, H.

(Citation)
Journal of Geophysical Research: Space Physics,123(2):1165-1177

(Issue Date)
2018-02

(Resource Type)
journal article

(Version)
Version of Record

AGU PUBLICATIONS

JGR

Journal of Geophysical Research: Space Physics

RESEARCH ARTICLE

10.1002/2017JA024801

Key Points:
- Dependence of the chorus generation on temperature anisotropy of energetic electrons is surveyed by self-consistent simulations
- Spectra of reproduced chorus conform estimations by the nonlinear theory but essentially different from those by the linear theory
- The necessary condition for the chorus generation is whether or not the amplitude of a triggering wave exceeds the threshold

Correspondence to:
Y. Katoh,
yuto@stpp.gp.tohoku.ac.jp

Citation:
Katoh, Y., Omura, Y., Miyake, Y., Usui, H., & Nakashima, H. (2018). Dependence of generation of whistler mode chorus emissions on the temperature anisotropy and density of energetic electrons in the Earth's inner magnetosphere. *Journal of Geophysical Research: Space Physics*, *123*, 1165–1177. https://doi.org/10.1002/2017JA024801

Received 28 SEP 2017
Accepted 17 JAN 2018
Accepted article online 23 JAN 2018
Published online 8 FEB 2018

Dependence of Generation of Whistler Mode Chorus Emissions on the Temperature Anisotropy and Density of Energetic Electrons in the Earth's Inner Magnetosphere

Y. Katoh[1], Y. Omura[2], Y. Miyake[3], H. Usui[3], and H. Nakashima[4]

[1]Department of Geophysics, Graduate School of Science, Tohoku University, Sendai, Japan, [2]Research Institute for Sustainable Humanosphere, Kyoto University, Kyoto, Japan, [3]Graduate School of System Informatics, Kobe University, Kobe, Japan, [4]Academic Center for Computing and Media Studies, Kyoto University, Kyoto, Japan

Abstract We carry out a series of self-consistent electron hybrid code simulations for the dependence of chorus generation process on the temperature anisotropy and density of energetic electrons in the Earth's inner magnetosphere. We use the same magnetic field gradient in the simulation system and different temperature anisotropy A_T for the initial distribution of energetic electrons at the magnetic equator. We conduct 6 sets of simulations for different A_T from 4 to 9, changing the initial number density N_h of energetic electrons at the equator in each set of simulations. By analyzing the spectra obtained in the simulation results, we identify chorus elements with rising tones in the results for higher N_h but no distinct chorus in smaller N_h. We compare the simulation results with estimations of the threshold and optimum amplitude proposed by the nonlinear wave growth theory. We find that the chorus generation processes reproduced in the simulation results are consistently explained by the theoretical estimates. We also compare the simulation results with linear growth rates for all simulation runs. We find clear disagreement between the spectral characteristics of reproduced chorus and the predictions by the linear theory. The present study clarifies that the spectra of chorus are essentially different from those predicted by the linear theory and are determined fully by nonlinear processes of wave-particle interactions in the chorus generation region.

1. Introduction

During a geomagnetically disturbed period, the population of energetic electrons in the Earth's inner magnetosphere increases due to enhanced magnetospheric convection and/or injection (e.g., Turner et al., 2015; Wang et al., 2008). The velocity distribution function of transported energetic electrons becomes anisotropic due to the conservation of the first adiabatic invariant, and the anisotropic electrons drive an instability generating a band of whistler mode waves (Kennel & Petschek, 1966; Summers et al., 2009, 2011), which play an important role in triggering the generation process of whistler mode chorus emissions. Chorus emissions are coherent electromagnetic plasma waves observed typically in the dawnside of the inner magnetosphere (Li et al., 2011; Macúšová et al., 2015; Tsurutani & Smith, 1974). They appear in dynamic spectra as a group of coherent wave elements with changing frequency in time (Kurita et al., 2012; Santolík et al., 2003, 2014). The typical frequency range is from 0.2 to 0.8 Ω_{e0}, where Ω_{e0} is the electron gyrofrequency at the magnetic equator, and a gap at 0.5 Ω_{e0} divides chorus into the upper band (0.5 to 0.8 Ω_{e0}) and the lower band (0.2 to 0.5 Ω_{e0}). Observations and simulations reveal that chorus show a variety of both spectral and propagation characteristics (e.g., Chen et al., 2013; Katoh, 2014; Li et al., 2012, 2016). Lower band chorus propagates mostly along magnetic field line in the equatorial region of the magnetosphere and becomes oblique in the region away from the equator. The wave normal angle of the upper band chorus is basically field aligned but is broadly distributed up to the resonance cone angle. Resonant wave-particle interactions occur between parallel propagating whistler mode waves and energetic electrons whose kinetic energy and pitch angle satisfy the cyclotron resonance condition. Landau resonance also occurs for obliquely propagating whistler mode waves. Previous studies revealed that wave-particle interactions associated with chorus play crucial roles in the evolution of radiation belt electrons (e.g., Jaynes et al., 2015; Turner et al., 2014) and in the precipitation of energetic electrons causing diffuse and pulsating aurora (e.g., Miyoshi et al., 2015; Ozaki et al., 2015; Thorne et al., 2010). The spatial distribution of chorus and its evolution including spectral properties is key information in understanding when/where/how wave-particle interactions take place in the magnetosphere, but conditions required for chorus generation have not been clarified yet. Properties of the generation mechanism of chorus

should be identified for understanding the interactions with energetic/relativistic electrons accurately. As has been surveyed by previous studies on the properties of very low frequency triggered emissions using the Vlasov Hybrid Simulation code (Nunn & Rycroft, 2005; Nunn et al., 2005), simulation studies of the chorus generation process should serve important clues on the properties of the chorus generation.

The generation process of chorus has been reproduced by a self-consistent particle code (e.g., Hikishima et al., 2009; Katoh & Omura, 2007, 2011, 2013, 2016; Omura et al., 2009, 2008), clarifying that chorus are generated through nonlinear wave-particle interactions occurring in the equatorial region of the magnetosphere. Omura et al. (2008, 2009) proposed the nonlinear wave growth theory for the generation mechanism of chorus with rising tones, and the theory can consistently explain both simulation results (Katoh & Omura, 2011, 2013) and observed properties of chorus (Kurita et al., 2012; Yagitani et al., 2014). Katoh and Omura (2013) showed that the magnetic field gradient along a field line controls the threshold amplitude required for chorus generation and suggested that chorus becomes hiss like when the threshold lowers significantly for a case of small magnetic field inhomogeneity. By assuming the same velocity distribution function of energetic electrons at the magnetic equator, they revealed that chorus appear in the simulation results of small spatial gradient of the background magnetic field but disappear for the largest gradient case assumed in their study. The largest gradient assumed in Katoh and Omura (2013) is the same condition used in Katoh and Omura (2011), who reported that chorus appears when they increased the number density of energetic electrons at the magnetic equator. In Katoh and Omura (2007, 2011, 2013), the same temperature anisotropy of energetic electrons has been assumed.

In the present study, we carry out a series of self-consistent electron hybrid simulations for the dependence of the chorus generation process on the temperature anisotropy and number density of energetic electrons. While numerous simulation runs are required for the investigation of the dependence, sufficient computational resources provided by both High-Performance Computing Infrastructure projects and collaborations with supercomputer centers of universities in Japan enable us to conduct the present study. We describe the simulation model and initial settings used in this study in section 2. Simulation results and properties of the chorus generation process revealed by the comparison with theoretical estimations are presented in section 3. Section 4 gives summary of the present study.

2. Simulation Model

We carry out simulations by using an electron hybrid code (e.g., Katoh & Omura, 2004, 2006; Katoh et al., 2005), which treats background cold electrons as a fluid and solves the motion of energetic electrons by the particle-in-cell method (Dawson, 1983). This code has been used for the investigation of the generation mechanism of chorus (Katoh & Omura, 2007, 2011, 2013, 2016; Omura et al., 2008, 2009). We use a spatially one-dimensional simulation system along a field line. The spatial gradient of the background magnetic field is an important factor controlling the threshold for the chorus generation (Katoh & Omura, 2013). In the present study, however, we use a spatial gradient 12.25 times larger than that of $L = 4$ of the dipole field, which is the same condition used in Katoh and Omura (2007, 2011). We use the large spatial gradient of the background magnetic field because we need to scale down the simulation system in order to reduce the computational time. It should be noted that the purpose of the present study is to discuss the physical process of the nonlinear wave-particle interaction itself rather than a direct comparison with observations in the real magnetosphere. The intensity of the background magnetic field assumed in the simulation system is the minimum at the center of the simulation system, corresponding to the magnetic equator, and grows when the distance h increases from the magnetic equator. We use 16,384 grid points with the grid spacing of 0.06 $c\Omega_{e0}^{-1}$ for the spatial extent of the simulation system $h = \pm 491.52\ c\Omega_{e0}^{-1}$ in both hemispheres away from the equator, where c is the speed of light. For the background magnetic field intensity at the magnetic equator of $L = 4$ (486 nT), 983.04 $c\Omega_{e0}^{-1}$ corresponds to 3,440.64 km (roughly 0.54 Earth radii). The time step is 0.01 Ω_{e0}^{-1}. We assume that the plasma frequency of cold electrons at the magnetic equator is 4 Ω_{e0} and that the number density of cold electrons N_0 is constant in both space and time.

The free energy in generating chorus is supplied by energetic electrons in the chorus generation region. In addition to a cold fluid component of electrons, we load 6.7×10^7 particles representing energetic electrons in the simulation system, taking into account the adiabatic motion along a field line, so as to realize the situation of the chorus generation region located at the equatorial region of the inner

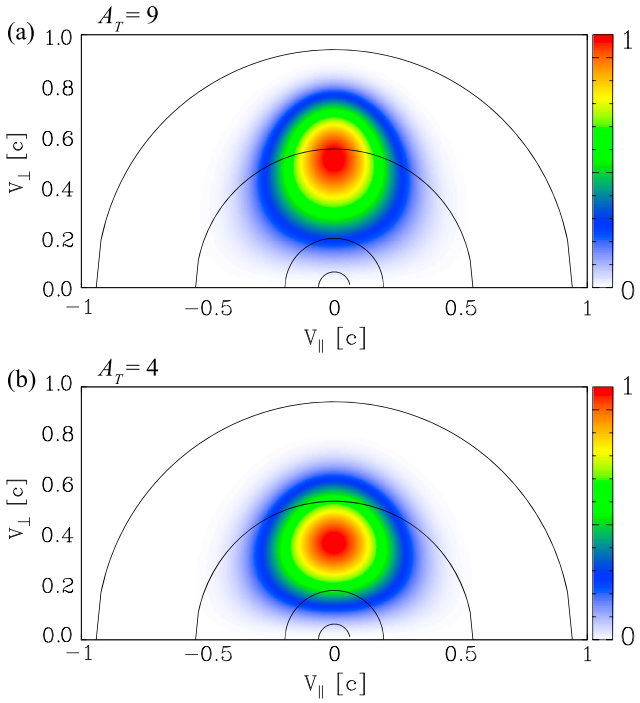

Figure 1. Initial velocity distributions of energetic electrons at the magnetic equator assumed in (a) Case 1 and (b) Case 6.

magnetosphere. We use the following equations for the initial distribution function of electrons in the momentum space:

$$f(u_\parallel, u_\perp) = C \exp\left(-\frac{u_\parallel^2}{2U_{t\parallel}^2}\right) g(u_\perp) \tag{1}$$

and

$$g(u_\perp) = \frac{1}{1-\beta}\left\{\exp\left(-\frac{u_\perp^2}{2U_{t\perp}^2}\right) - \exp\left(-\frac{u_\perp^2}{2\beta U_{t\perp}^2}\right)\right\}, \tag{2}$$

where C is a constant and $u_\parallel$ and $u_\perp$ are momenta parallel and perpendicular to the background magnetic field, respectively. The parameters $U_{t\parallel}$ and $U_{t\perp}$ are thermal momenta parallel and perpendicular to the background magnetic field, respectively, and β is a parameter describing the depth of the loss cone distribution, and we use $\beta = 0.5$. The temperature anisotropy A_T is computed by $A_T = (1+\beta)U_{t\perp}^2/U_{t\parallel}^2 - 1$ (cf. Tang et al., 2014). In the present study, for the investigation of the dependence of the chorus generation process on the kinetic energy of anisotropic electrons, we carry out 6 sets of simulations from Case 1 to Case 6 for different A_T. We assume that $A_T = 9$ in Case 1 and decrease A_T every case down to 4 in Case 6. Figure 1 shows the initial distribution of energetic electrons in the velocity phase space: Figure 1a for $A_T = 9$ (Case 1) and Figure 1b for $A_T = 4$ (Case 6). The initial parameters used in each set of simulations are summarized in Table 1. We assume that the same parameter $U_{t\parallel}/c = 0.194$ for all runs and vary $U_{t\perp}/c$ to change the temperature anisotropy A_T. In each set of simulations, we conduct a series of simulation runs with the same A_T but with a different initial number density of energetic electrons N_h at the magnetic equator ($h = 0$), as given in Table 2, in order to determine the parameters which lead to distinct chorus in simulation results. We carry out every simulation longer than 10,000 Ω_{e0}^{-1} so as to study whether or not chorus is generated under the assumed initial parameters.

For efficient computation of many simulation runs, we used a newly developed electron hybrid code domain decomposed by OhHelp (Katoh et al., 2016; Nakashima et al., 2009) as well as a conventional particle-decomposed electron hybrid code. The OhHelp is a library enables us to conduct particle-in-cell simulations by achieving both dynamic load balancing and scalability in massively parallel computing systems. The improved electron hybrid code shows the linear scalability up to thousands of message passing interface (MPI) processes. While we used almost 3 days with 256 cores of supercomputer for each run by the parallel-decomposed code, the computational efficiency of the code is improved and becomes significantly better with an increase in the number of cores used in the simulation (Katoh et al., 2016), 50% with 256 cores and 106% with 1,024 cores.

3. Results and Discussion

We carried out a series of electron hybrid simulations and analyzed spectra in simulation results for the generation of chorus elements with rising tones. As a typical example of simulation results, we show in Figure 2 the time series of the spatial distribution of wave magnetic field spectra obtained in the simulation result of Run 2 of Case 1. The sequence of the generation process of chorus reproduced in the simulation result is consistent with previous studies (e.g., Katoh & Omura, 2007, 2011; Omura et al., 2008, 2009) and is briefly summarized as follows. In the early stage of the simulation result (Figure 2a), a band of whistler mode waves are generated through an instability driven by the temperature anisotropy assumed in the initial velocity distribution function of energetic electrons. The amplitude of whistler mode waves increases during their propagation (Figure 2b). Coherent wave elements with rising tones appear in the spectra in the region close to the magnetic equator

Table 1
Initial Parameters for the Distribution of Energetic Electrons at the Magnetic Equator Used in Each Set of Simulations of Each Case

	A_T	$U_{t\parallel}/c$	$U_{t\perp}/c$
Case 1	9	0.194	0.501
Case 2	8	0.194	0.475
Case 3	7	0.194	0.448
Case 4	6	0.194	0.419
Case 5	5	0.194	0.388
Case 6	4	0.194	0.354

Table 2
Number Density of Energetic Electrons N_h at the Equator (h = 0) Assumed in Each Run, Normalized by the Number Density of Cold Electrons N_0

	Case 1	Case 2	Case 3	Case 4	Case 5	Case 6
Run 1	8.22×10^{-4}	8.78×10^{-4}	8.50×10^{-4}	1.22×10^{-3}	1.22×10^{-3}	1.51×10^{-3}
Run 2	7.47×10^{-4}	8.04×10^{-4}	7.80×10^{-4}	1.09×10^{-3}	1.18×10^{-3}	1.38×10^{-3}
Run 3	6.72×10^{-4}	7.31×10^{-4}	7.10×10^{-4}	9.60×10^{-4}	1.14×10^{-3}	1.26×10^{-3}
Run 4	5.98×10^{-4}	6.55×10^{-4}	6.38×10^{-4}	8.80×10^{-4}	1.11×10^{-3}	1.13×10^{-3}
Run 5	-	5.83×10^{-4}	5.67×10^{-4}	8.20×10^{-4}	1.08×10^{-3}	1.00×10^{-3}
Run 6	-	-	-	7.50×10^{-4}	1.05×10^{-3}	8.80×10^{-4}
Run 7	-	-	-	6.80×10^{-4}	9.15×10^{-4}	-
Run 8	-	-	-	5.50×10^{-4}	7.80×10^{-4}	-

(Figure 2c), and the rising tone elements grow nonlinearly during their propagation away from the equator (Figures 2c and 2d).

Figure 3 shows wave magnetic field spectra obtained at h = 98.3 $c\Omega_{e0}{}^{-1}$ in Case 1, in which we assumed A_T = 9 and different N_h at the magnetic equator. Figure 3a is the result of Run 1 we showed in Figure 2. Chorus elements with rising tones appear in Figures 3a–3c, and the number of elements increases with increasing N_h. In contrast, distinct chorus elements did not appear in Figure 3d. Figure 4 shows the velocity distribution of energetic electrons in the simulation result of Run 3 (Figure 3c) at t = 12,000 $\Omega_{e0}{}^{-1}$, corresponding to the timing after the generation of chorus elements with rising tones. We find in Figure 4 that the velocity distribution is modified due to the pitch angle scattering occurring in the chorus generation process, as studied by Hikishima et al. (2010). Figure 5 shows the simulation results of Case 6, where we assumed A_T = 4. Chorus elements with rising tones are clearly identified in the spectra shown in Figures 5a and 5b. In

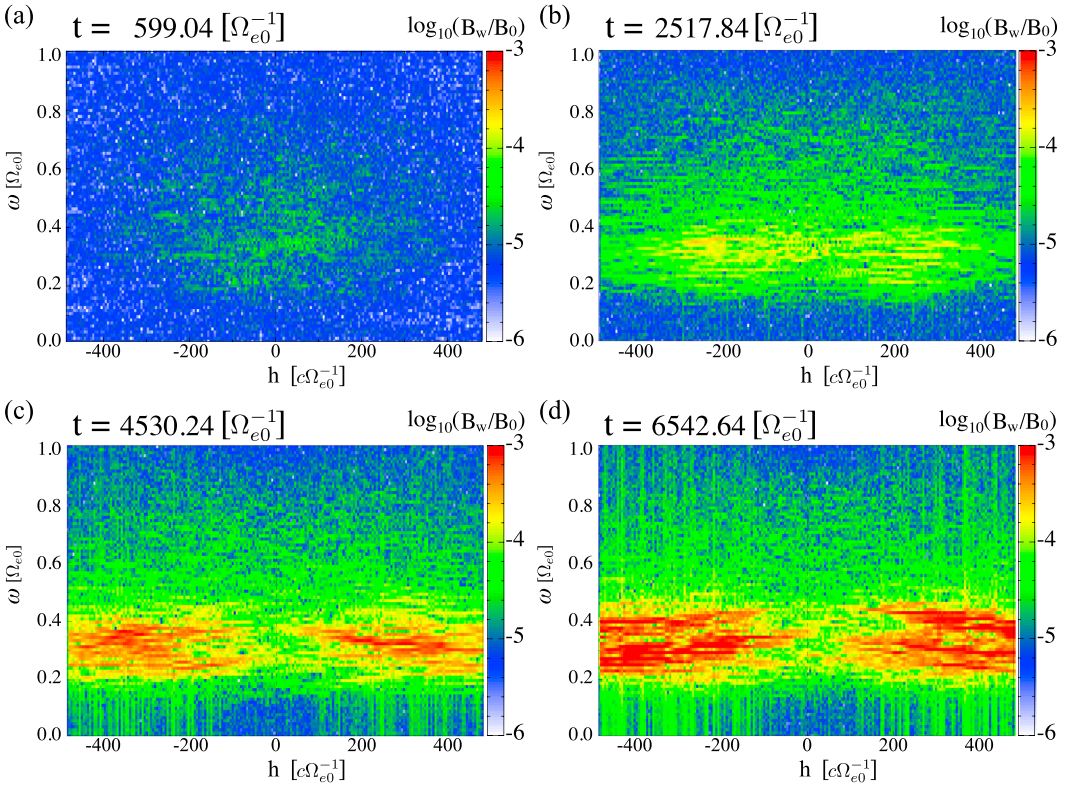

Figure 2. Spatial profiles of the spectra of the wave magnetic field at (a) t = 599.04 $\Omega_{e0}{}^{-1}$, (b) 2517.84 $\Omega_{e0}{}^{-1}$, (c) 4530.24 $\Omega_{e0}{}^{-1}$, and (d) 6542.64 $\Omega_{e0}{}^{-1}$ in Run 1 of Case 1.

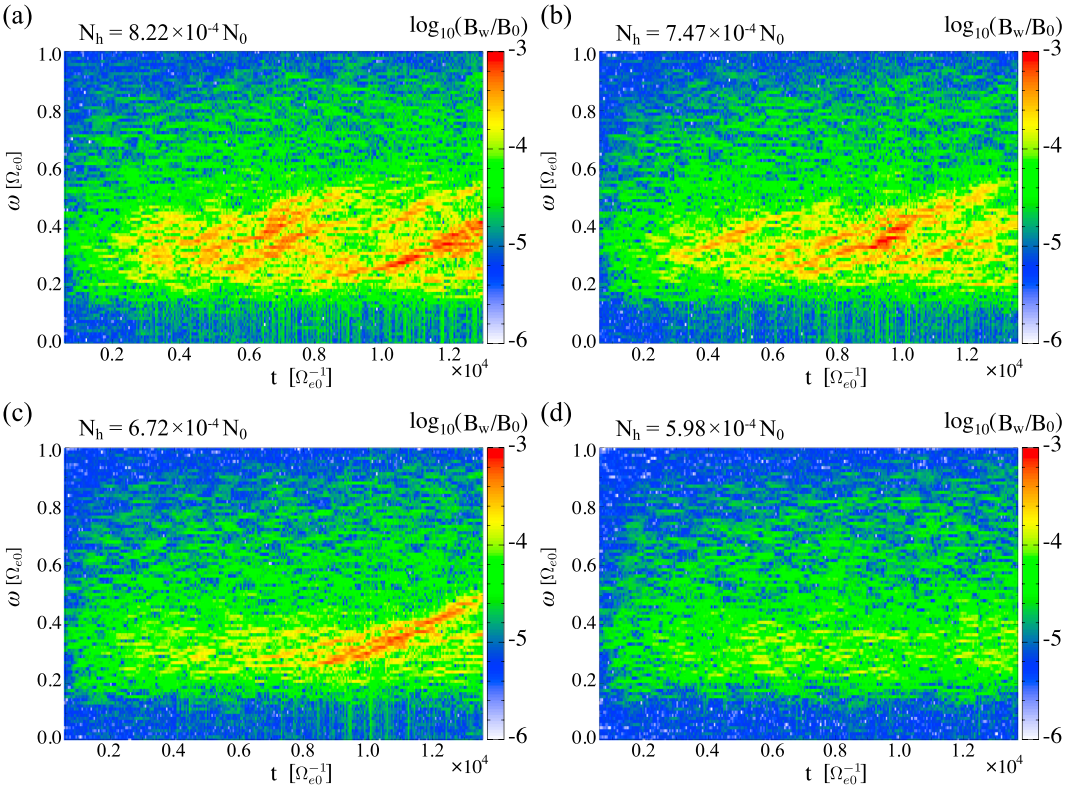

Figure 3. Dynamic spectra of the wave magnetic field at a fixed point (h = 98.30 $c\Omega_{e0}^{-1}$) in (a) Run 1, (b) Run 2, (c) Run 3, and (d) Run 4 of Case 1.

Figure 5c, we can recognize relatively large-amplitude wave components appearing in the latter half of the simulation ($t > 10^4\ \Omega_{e0}^{-1}$) and a slight frequency variation of waves, but the amount of the frequency shift is not as significant as we find in Figures 5a and 5b. We also identify in Figure 5d a band of whistler mode waves but no distinct rising tone emissions. As shown in Figures 3 and 5, we find that initial conditions suitable for the chorus generation are captured in the sets of parameters assumed in the present study.

We compare the simulation results with estimations of the threshold (Omura et al., 2009) and optimum amplitude (Omura & Nunn, 2011) based on the nonlinear wave growth theory. The equation of the threshold Ω_{th} is given by

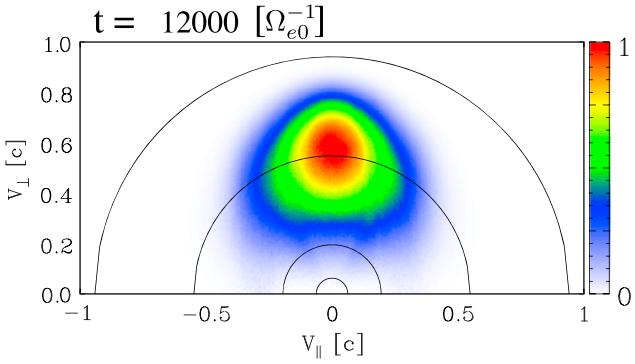

Figure 4. Velocity distribution of energetic electrons in the simulation result of Run 3 of Case 1 (Figure 3c) at t = 12,000 Ω_{e0}^{-1}, corresponding to the timing after the chorus generation.

$$\widetilde{\Omega}_{th} = \frac{100\pi^3\gamma^3\xi}{\widetilde{\omega}\widetilde{\omega}_{ph}^4\widetilde{V}_{\perp0}^5\chi^5}\left(\frac{\widetilde{a}s_2\widetilde{U}_{t\parallel}}{Q}\right)^2 \exp\left(\frac{\gamma^2\widetilde{V}_R^2}{\widetilde{U}_{t\parallel}^2}\right), \quad (3)$$

where $\widetilde{\Omega}_{th} = \Omega_{th}/\Omega_{e0}$, γ is the Lorentz factor, $\xi^2 = \omega(\Omega_e - \omega)/\omega_{pe}^2$, $\widetilde{\omega} = \omega/\Omega_{e0}$, $\widetilde{\omega}_{ph} = \omega_{ph}/\Omega_{e0}$, $\omega_{ph} = \omega_{pe}(N_h/N_0)^{1/2}$, $\widetilde{V}_{\perp0} = V_{\perp0}/c$, $V_{\perp0}$ is an average value of the perpendicular component of the velocity of energetic electrons, $\chi = (1+\xi^2)^{-1/2}$, and $\widetilde{a} = ac^2/\Omega_{e0}^2$. In the above equation,

$$s_2 = \frac{1}{2\xi\chi}\left\{\frac{\gamma\omega}{\Omega_e}\left(\frac{V_{\perp0}}{c}\right)^2 - \left[2 + \Lambda\frac{\chi^2(\Omega_e - \gamma\omega)}{\Omega_e - \omega}\right]\frac{V_R V_p}{c^2}\right\}, \quad (4)$$

Λ is a parameter describing the variation of the background plasma density along a field line and Λ = 1 in the present study, V_R is the resonance velocity, V_p is the phase velocity, $\widetilde{U}_{t\parallel} = U_{t\parallel}/c$, $\widetilde{V}_R = V_R/c$, and Q

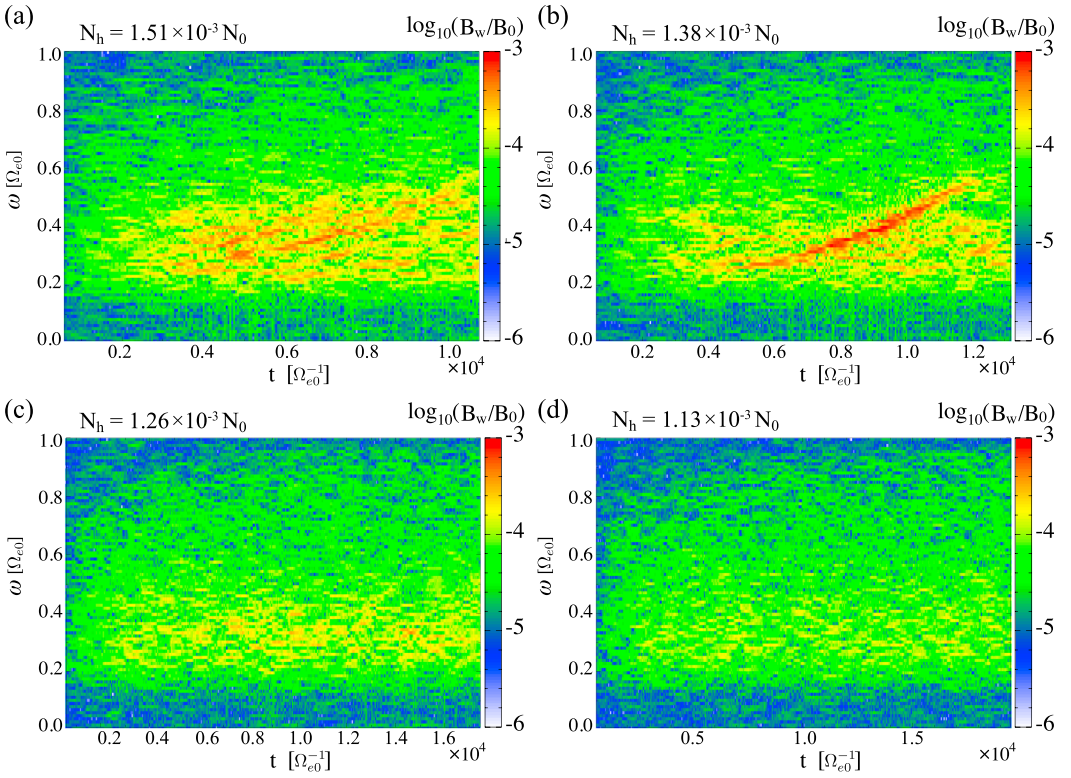

Figure 5. Dynamic spectra of the wave magnetic field at a fixed point (h = 98.30 $c\Omega_{e0}{}^{-1}$) in (a) Run 1, (b) Run 2, (c) Run 3, and (d) Run 4 of Case 6.

represents the depth of the electromagnetic electron hole in the velocity phase space. The optimum wave amplitude Ω_{opt} is given by

$$\widetilde{\Omega}_{opt} = 0.81\pi^{-5/2}\frac{Q}{\tau}\frac{s_1\widetilde{V}_g}{s_0\widetilde{\omega}\widetilde{U}_{t\parallel}}\left(\frac{\widetilde{\omega}_{ph}\widetilde{V}_{\perp 0}}{\gamma}\right)^2 \exp\left(-\frac{\gamma^2\widetilde{V}_R^2}{2\widetilde{U}_{t\parallel}^2}\right), \tag{5}$$

where $\widetilde{\Omega}_{opt} = \Omega_{opt}/\Omega_{e0}$,

$$s_0 = \frac{\chi}{\xi}\frac{V_{\perp 0}}{c}, s_1 = \gamma\left(\frac{1-V_R}{V_g}\right)^2 \tag{6}$$

τ is the ratio of the nonlinear transition time T_N to the nonlinear trapping period T_{tr} (cf. Omura & Nunn, 2011). Figure 6 indicates the maximum wave magnetic field amplitude as a function of wave frequency obtained at h = 0. We also show in Figure 6 the estimated threshold and optimum amplitudes for each run. We estimated Ω_{th} and Ω_{opt} using the initial condition assumed in each run, while we assumed Q = 0.5 and τ = 0.25.

Figure 6a is the results of Case 1, which we showed the spectra in Figure 3. Black, red, green, and blue lines in Figure 6a indicate the results of Run 1, Run 2, Run 3, and Run 4, respectively. Solid, dashed, and dotted lines are simulation results, estimated threshold, and optimum amplitudes, respectively. As shown in Figure 3, distinct chorus with rising tones appeared in Runs 1–3 of Case 1 but no distinct chorus in Run 4. The presence of chorus is clearly identified in Figure 6a as well; the wave amplitudes of Runs 1–3 in the frequency range from 0.3 Ω_{e0} to 0.6 Ω_{e0} corresponding to chorus elements are significantly larger than that of Run 4. We find in Figure 6a that the threshold lowers with decreasing N_h and that the wave amplitudes obtained in Runs 1–3 significantly exceed the threshold in the frequency range of the chorus elements. On the other hand, the amplitude obtained in Run 4 is close to the threshold, especially in the frequency range around 0.3 Ω_{e0}, implying that the wave amplitude around the equator in Run 4 was not enough to trigger the generation of rising tone chorus, and therefore, we did not see distinct chorus in Run 4. In

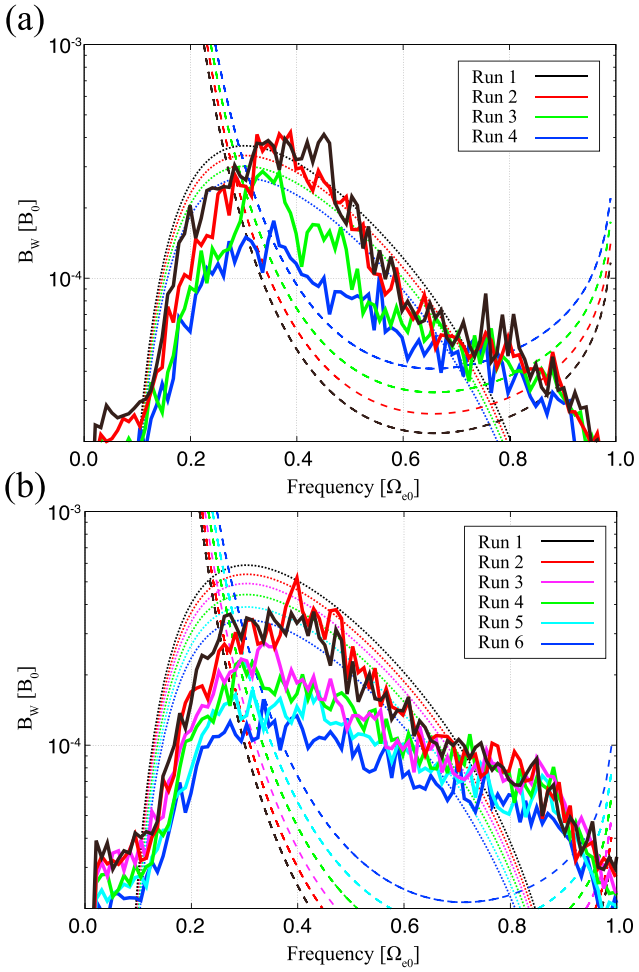

Figure 6. The maximum wave magnetic field amplitudes of the frequency spectra at the magnetic equator (h = 0) obtained throughout each of the simulation runs in (a) Runs 1–4 of Case 1 and (b) Runs 1–6 of Case 6 plotted with solid colored lines. The threshold and optimum amplitudes for the nonlinear wave growth are, respectively, plotted with dashed and dotted lines of the corresponding colors. We assumed τ = 0.25 in calculating the optimum wave amplitudes.

addition, we find in Figure 6a that the profiles of the wave amplitude of Runs 1 and 2 as a function of the frequency conform to the estimated profiles of the optimum amplitude.

We show the results of Case 6 in Figure 6b with the same format as we used in Figure 6a. Sold lines are the maximum wave magnetic field amplitude of the frequency spectra at the magnetic equator (h = 0) obtained in Runs 1–6 of Case 6. The threshold and optimum amplitudes for the nonlinear wave growth are plotted with dashed and dotted lines of the corresponding colors, respectively. By comparing Figure 6b with Figure 6a, we find that the threshold lowers in Case 6 than those in Case 1, because of the small A_T assumed in Case 6. Distinct chorus elements appeared in Runs 1 and 2 of Case 6, as shown in Figure 5. Figure 6b reveals that the wave amplitudes in Runs 1 and 2 are significantly larger than those of other runs and exceed the estimated threshold amplitudes in the frequency range around 0.3 Ω_{e0}, corresponding to the starting frequency of the chorus elements appeared in the spectra. Also, the frequency profiles of the wave amplitude of Runs 1 and 2 conform the profiles of the optimum amplitude. We conducted the same analysis on other sets of simulations (Cases 2–5) and found the consistency between the simulation results with the estimations of both threshold and optimum amplitudes. Based on the results of the comparison, we conclude that the generation process of chorus elements reproduced in the simulation results is consistently explained by the nonlinear wave growth theory.

The simulation results of the present study reveal that the chorus generation process is governed fully by nonlinear processes of wave-particle interactions. In Figure 7, we show the spectra obtained in the simulation results (Figures 7b, 7d, 7f, 7h, 7j, and 7l for Cases 1, 2, 3, 4, 5, and 6, respectively) and linear growth rates of whistler mode waves estimated by the linear theory of Xiao et al. (1998) for the initial condition of energetic electrons at the magnetic equator (Figures 7a, 7c, 7e, 7g, 7i, and 7k for Cases 1, 2, 3, 4, 5, and 6, respectively). Both simulation results and linear growth rates are presented in Figure 7 as a function of N_h. The significance of the nonlinear process becomes evident in the cases with larger N_h. First, we examine Figures 7a and 7b for Case 1. Figure 7a indicates that the linear growth rate is positive in the frequency range corresponding to the lower band chorus and that the growth rate increases with increasing N_h, while the maximum growth rate is obtained at 0.27 Ω_{e0}. By comparing Figure 7a with Figure 7b, we find that the frequency coverage and the frequency of the peak amplitude of enhanced emissions found in the simulation results of lower N_h are basically consistent with those predicted by the linear theory. On the other hand, the wave amplitude becomes large for higher N_h runs and the frequency range of the enhanced emissions expands to the higher-frequency range up to 0.6 Ω_{e0}, indicating that the spectra deviate from the predictions by the linear theory. Since chorus with rising tones appeared in the spectra for higher N_h (Runs 1–3 of Case 1) but no distinct chorus in smaller N_h (Run 4 of Case 1) as we discussed in Figures 3 and 6a, we find that the enhancement of the spectra shown in Figure 7b indicates the presence of chorus elements with rising tones. Next, we study the results of other cases and find that the deviation of the spectra from the linear theory under the presence of chorus emissions is clearly recognized in each case (Figures 7c–7l). Moreover, Figure 7 reveals that the difference becomes more significant for smaller A_T cases. While the decrease of A_T results in the decrease of the linear growth rates (Figures 7a, 7c, 7e, 7g, 7i, and 7k), the wave amplitude under the presence of chorus does not change significantly. The maximum linear growth rate is 1.31×10^{-3} Ω_{e0} at 0.27 Ω_{e0} in Run 1 of Case 1 and becomes 5.42×10^{-4} Ω_{e0} at 0.28 Ω_{e0} in Run 1 of Case 6, whereas the wave amplitude of chorus reproduced in the simulation results is in the same level over 3.0×10^{-4} B_0 and is basically unchanged in each run. The discrepancy between the variation of

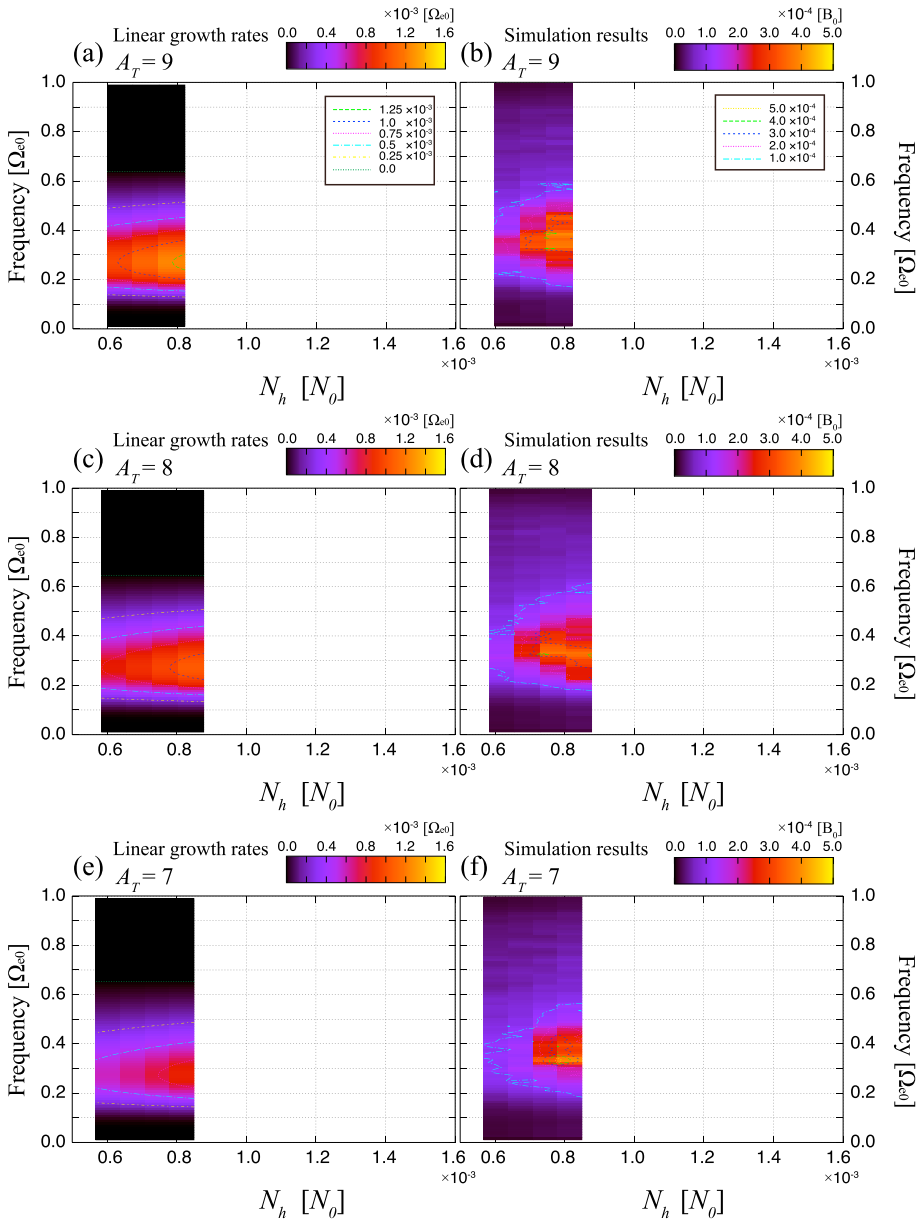

Figure 7. Linear growth rates of whistler mode waves estimated by the linear theory of Xiao et al. (1998) for the initial condition of energetic electrons at the magnetic equator (a, c, e, g, i, and k for Cases 1, 2, 3, 4, 5, and 6, respectively) and the wave magnetic field spectra obtained in the simulation results (b, d, f, h, j, and l for Cases 1, 2, 3, 4, 5, and 6, respectively).

the linear growth rates and the chorus intensity can be explained by the optimum amplitude (Omura & Nunn, 2011) based on the nonlinear wave growth theory; after the triggering of chorus elements, the wave generation mechanism switches into the nonlinear stage and then the spectra follow the profile determined by fully nonlinear processes that is independent of the linear growth rate in the early stage of the simulation. Based on the results shown in Figure 7, we conclude that the spectra of chorus are essentially different from those predicted by the linear theory and are determined by fully nonlinear processes of wave-particle interactions in the chorus source region.

By conducting a series of electron hybrid code simulations, we revealed parameters suitable for the chorus generation under the initial settings of the simulation system. Figure 8 shows the summary of simulations

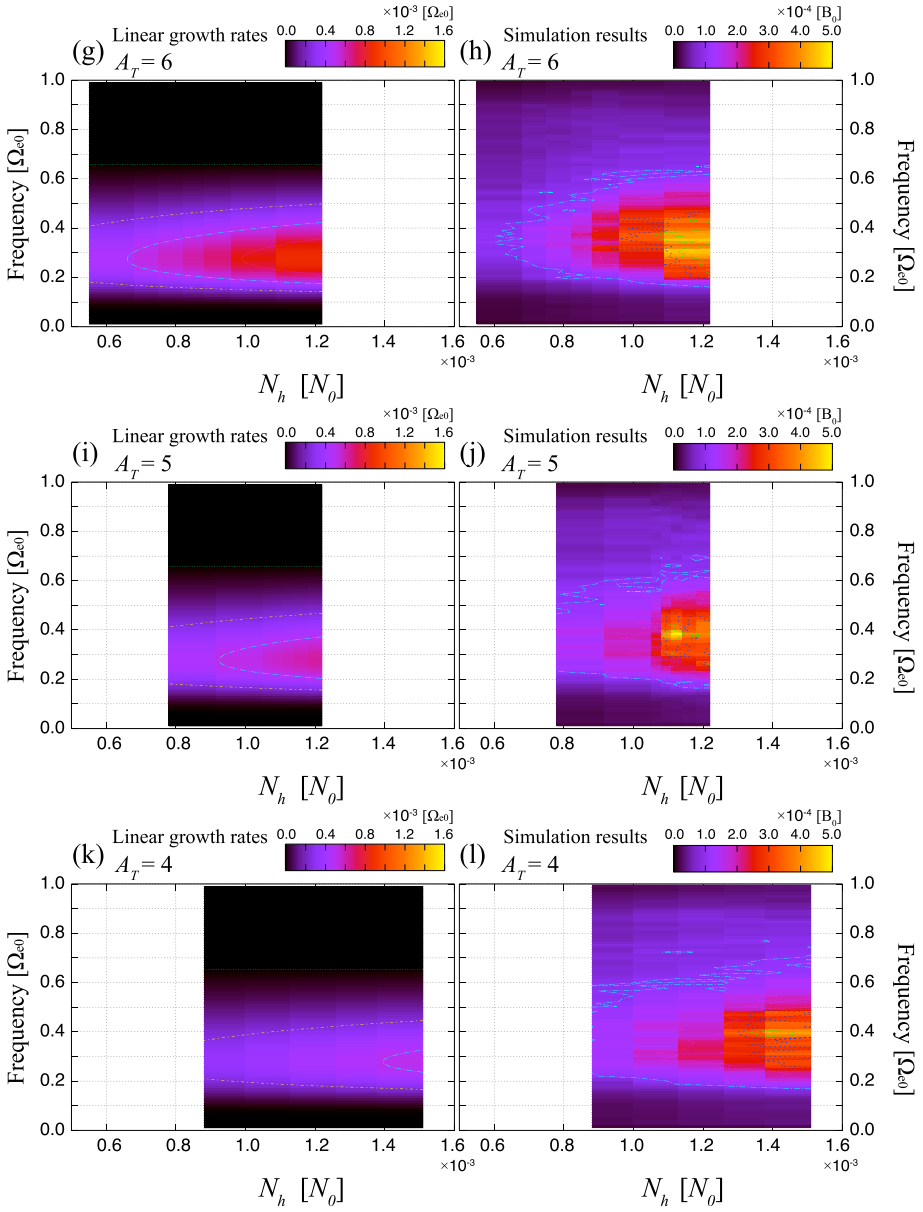

Figure 7. (continued)

carried out in the present study. Red filled circles indicate initial N_h and A_T values for which we identified distinct chorus, whereas blue open circles represent sets of parameters for which we did not find distinct chorus in the simulation results. Figure 8 demonstrates how the conditions required for the chorus generation vary depending on the initial N_h and A_T; higher N_h is required for the generation of distinct chorus in smaller A_T. Since we assumed the same parameter $U_{t\parallel}/c = 0.194$ for all runs, the variation of the temperature anisotropy A_T in the present study is equivalent to the change of $U_{t\perp}/c$. This tendency recalls the characteristics of the linear growth rate that high N_h should be required to obtain a certain level of the growth rate for smaller A_T, but Figure 7 clarified the nonlinear nature of the chorus generation and revealed that the spectral characteristics of chorus are essentially different from the predictions of the linear theory. Indeed, the linear theory is useful to predict the evolution of a band of whistler mode waves excited in the early stage of the simulation, in which we identified a band of whistler mode waves generated through an instability driven by the temperature anisotropy, but is not enough to understand

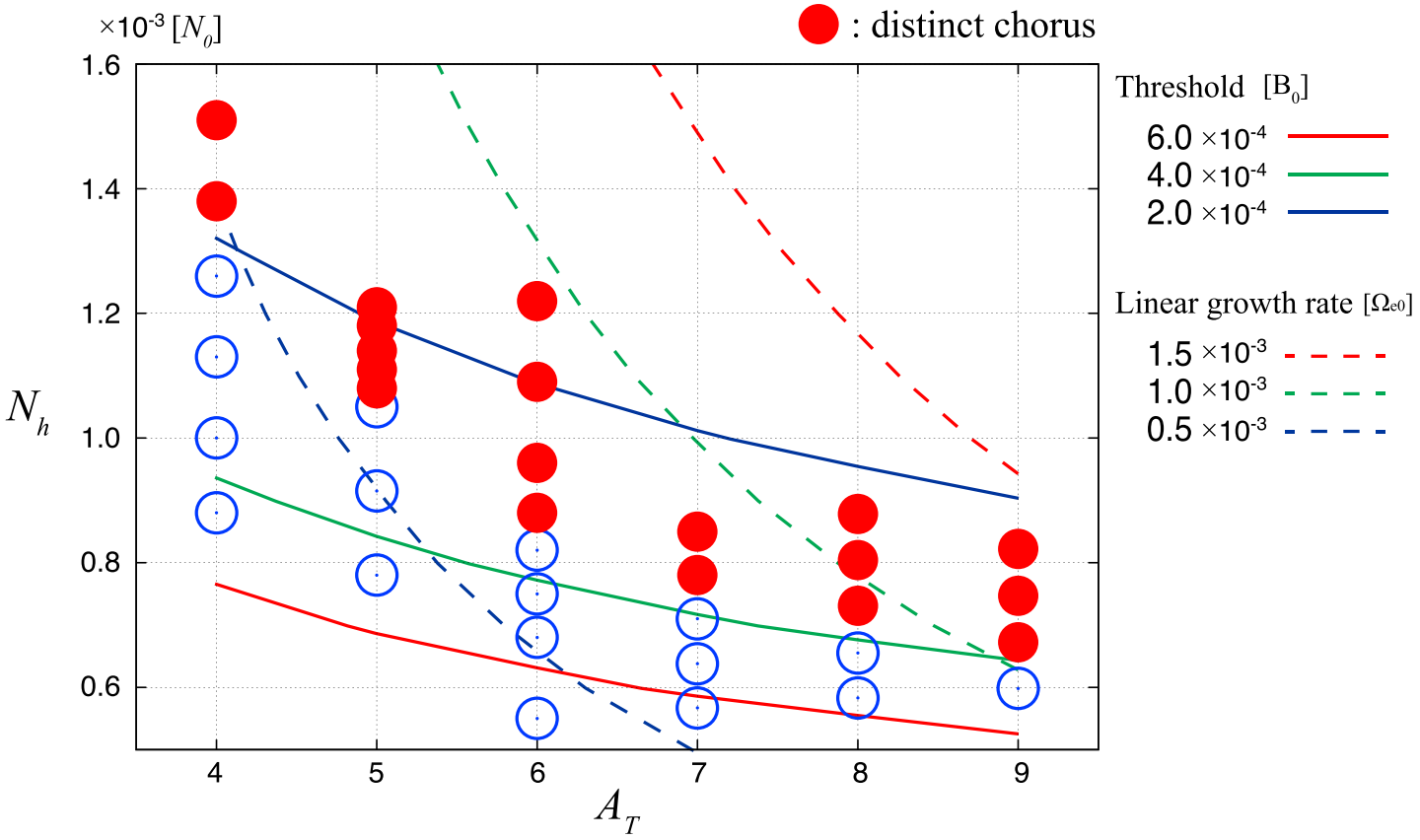

Figure 8. Summary of the simulations carried out in the present study. Red filled circles indicate initial N_h and A_T values with which we found distinct chorus, whereas blue open circles represent the set of the parameters with which we did not find distinct chorus in the simulation results. Solid and dashed lines represent contours of the threshold amplitude and the maximum linear growth rate, respectively, estimated with the corresponding parameters of N_h and A_T values.

the generation process of chorus. While the amplitudes of the generated whistler mode waves grow in time during their propagation in the equatorial region of the simulation system, when the amplitude exceeds the threshold, the waves grow locally as an absolute instability with increasing frequencies and then chorus emissions with rising tones emerge from the region close to the magnetic equator. Therefore, the necessary condition for the chorus generation is not the magnitude of the linear growth rate itself but whether the wave amplitude exceeds the threshold or not. We note that the threshold lowers with decreasing the temperature anisotropy, as indicated in Figure 5, and thereby, the condition for chorus generation is determined by the balance between the threshold and wave amplitude of triggering waves. The boundary between red filled circles and blue open circles in Figure 8 indicates the conditions where the amplitude of triggering waves exceeds the threshold under the initial conditions used in the simulations.

Solid and dashed lines in Figure 8 represent contours of the threshold amplitude and the maximum linear growth rate, respectively, estimated with the corresponding parameters of N_h and A_T values. Figure 8 shows that the boundary varies between the contours of the threshold amplitude and linear growth rate. The boundary is close to the contour of the threshold amplitude $4.0 \times 10^{-4}\ B_0$ for $A_T = 9$, where the linear growth rate is relatively high ($1.0 \times 10^{-3}\ \Omega_{e0}$), and gradually deviates from the contour toward the smaller threshold amplitude $2.0 \times 10^{-4}\ B_0$ for $A_T = 4$, where the linear growth rate is relatively small ($0.5 \times 10^{-3}\ \Omega_{e0}$). The tendency revealed by Figure 8 can be explained by the relation between the threshold amplitude and the spatial extent of the wave generation region. The spatial extent of the wave generation region is limited around the magnetic equator, because the mirror force acting on particles becomes large in the region away from the equator due to the spatial gradient of the background magnetic field. Since we used the same spatial gradient of the background magnetic field in the present study, the spatial extent of the wave generation region is the same for all simulation runs. For the large A_T cases with larger linear growth

rates, triggering waves can achieve amplitudes greater than the threshold during their propagation in the wave generation region, and therefore, chorus can be generated in the condition corresponding to the relatively high threshold amplitude. On the other hand, for the smaller A_T cases with smaller linear growth rates, the amplitudes of triggering waves become smaller, and thereby, chorus emissions can only be generated under the smaller threshold conditions.

Omura and Nunn (2011) derived the optimum amplitude at which the nonlinear wave growth of a chorus element becomes most effective. While the discussion of the threshold corresponds to the triggering process of a chorus element with a rising tone, the discussion of the optimum amplitude corresponds to the nonlinear process occurring after the triggering of a chorus element. In the derivation of the optimum amplitude (5), it is essential to consider the role of J_B, which is the component of nonlinear resonant currents parallel to the wave magnetic field vector. The presence of J_B results in the frequency change of triggered waves. The optimum amplitude gives the condition under which the amount of the frequency change due to J_B maximizes the magnitude of the resonant current J_E, where J_E is the component of resonant currents parallel to the wave electric field vector, contributing to the nonlinear growth of the wave amplitude. While the presence of a coherent wave with a finite wave amplitude is assumed in the discussion of J_E and J_B, the present study clarified the condition of the chorus emissions from spontaneously generated whistler mode waves through the instability driven by a temperature anisotropy. The consistency between the simulation results and theoretical estimations revealed that the properties of chorus are determined fully by nonlinear processes of wave-particle interactions. In a case of an isotropic velocity distribution of energetic electrons, we do not expect the generation of chorus because we do not expect the emergence of a triggering wave from thermal fluctuations. As suggested by previous studies (e.g., Omura et al., 2009; Omura & Nunn, 2011), a triggering wave whose wave amplitude is larger than the threshold is required for the triggering of a chorus element with rising tones. If there is no triggering wave, the magnitudes of both J_E and J_B become negligible.

We used (1) and (2) for the initial distribution of energetic electrons in the simulation system. While the simplified distribution as described by equations (1) and (2) is useful in understanding fundamental physics of wave-particle interactions, simulations with the plasma environment and velocity distributions observed in the real magnetosphere are also important for the thorough understanding of the chorus generation process. Recently, the Arase (ERG) satellite (Miyoshi et al., 2012) started to serve a new set of in situ observation of plasma waves (e.g., Kasahara, Yokota, et al., 2018; Katoh et al., 2018) and particles (e.g., Kazama et al., 2017; Kasahara, Kasaba, et al., 2018) in the inner magnetosphere. Simulations with the initial condition corresponding to the Arase observation should contribute to the physical interpretation of the observed properties of whistler mode chorus. Such works are important in our future study.

4. Summary

To study the dependence of the chorus generation process on the temperature anisotropy and density of energetic electrons, we carried out a series of self-consistent electron hybrid code simulations with the same magnetic field gradient in the simulation system. We assumed different temperature anisotropies A_T for initial distribution of energetic electrons at the magnetic equator. We carried out 6 sets of simulations for different A_T from 4 to 9 and changed the initial number density N_h of energetic electrons at the equator in each set of simulations. Since we assumed the same parameter $U_{t\parallel}/c = 0.194$ for all runs, the variation of the temperature anisotropy A_T in the present study is equivalent to the change of $U_{t\perp}/c$. We analyzed spectra in the simulation results showing generation of chorus elements with rising tones and found the sets of initial parameters suitable for chorus generation. Chorus emissions with rising tones are found in the simulation with higher N_h but no distinct chorus is generated with smaller N_h. We compared the simulation results with estimations of the threshold (Omura et al., 2009) and optimum amplitudes (Omura & Nunn, 2011) and found that the simulation results are consistently explained by the nonlinear wave growth theory. We also compared the simulation results with estimated linear growth rates for all simulation runs and found distinct discrepancy between the spectral characteristics of chorus reproduced in the simulation results and the predictions by the linear theory. The wave amplitude becomes large for higher N_h runs, and the frequency range of the enhanced emissions expands to the higher-frequency range up to 0.6 Ω_{e0}, indicating that the spectra deviate from the predictions by the linear theory.

Based on the simulation results and the results of analysis, we concluded that the spectra of chorus are essentially different from those predicted by the linear theory and are determined fully by nonlinear processes of wave-particle interactions in the chorus generation region. The results of the present study revealed that the necessary condition for chorus generation is not the magnitude of the linear growth rate itself but whether or not the wave amplitude exceeds the threshold amplitude, which is controlled by the magnetic field gradient, number density of energetic electrons, and their temperature anisotropy.

Acknowledgments
The computer simulation was performed on the KDK computer system at the Research Institute for Sustainable Humanosphere, Kyoto University, and the computational resources of the HPCI system provided by the Research Institute for Information Technology, Kyushu University; the Information Technology Center, Nagoya University; and the Cyberscience Center, Tohoku University through the HPCI System Research Project (Project IDs: hp160131 and hp170064). This study is supported by Grants-in-Aid for Scientific Research (26287120, 15H05747, 15H05815, 15H03730, 17K18798, and 17H06140) of Japan Society for the Promotion of Science. This research is also supported by "Advanced Computational Scientific Program" of Research Institute for Information Technology, Kyushu University, by "Joint Usage/Research Center for Interdisciplinary Large-scale Information Infrastructures" in Japan (Project ID: jh170005-NAH), by MEXT as "Exploratory Challenge on Post-K computer" (Elucidation of the Birth of Exoplanets (Second Earth) and the Environmental Variations of Planets in the Solar System), and by "Computational Joint Research Program (Collaborative Research Project on Computer Science with High-Performance Computing)" at the Institute for Space-Earth Environmental Research, Nagoya University. We thank D. Summers for useful discussions. The simulation data supporting this paper are available upon request to the corresponding author.

References

Chen, L., Thorne, R. M., Li, W., & Bortnik, J. (2013). Modeling the wave normal distribution of chorus waves. *Journal of Geophysical Research: Space Physics*, *118*, 1074–1088. https://doi.org/10.1029/2012JA018343

Dawson, J. M. (1983). Particle simulation of plasmas. *Reviews of Modern Physics*, *55*(2), 403–447. https://doi.org/10.1103/RevModPhys.55.403

Hikishima, M., Yagitani, S., Omura, Y., & Nagano, I. (2009). Full particle simulation of whistler-mode rising chorus emissions in the magnetosphere. *Journal of Geophysical Research*, *114*, A01203. https://doi.org/10.1029/2008JA013625

Hikishima, M., Omura, Y., & Summers, D. (2010). Microburst precipitation of energetic electrons associated with chorus wave generation. *Geophysical Research Letters*, *37*, L07103. https://doi.org/10.1029/2010GL042678

Jaynes, A. N., Baker, D. N., Singer, H. J., Rodriguez, J. V., Loto'aniu, T. M., Ali, A. F., … Reeves, G. D. (2015). Source and seed populations for relativistic electrons: Their roles in radiation belt changes. *Journal of Geophysical Research: Space Physics*, *120*, 7240–7254. https://doi.org/10.1002/2015JA021234

Kasahara, S., Yokota, S., Mitani, T., Aasamura, K., Hirahara, M., Shibano, Y., & Takashima, T. (2018). Medium-energy particle experiments–electron analyser (MEP-e) for the exploration of energization and radiation in geospace (ERG) mission. *Earth, Planets and Space*, *70*. https://doi.org/10.1186/10.1186/s40623-017-0752-x

Kasahara, Y., Kasaba, Y., Kojima, H., Yagitani, S., Ishisaka, K., Kumamoto, A., … Shinohara, I. (2018). The Plasma Wave Experiment (PWE) on board the Arase (ERG) satellite. *Earth, Planets and Space*, *70*. https://doi.org/10.1186/s40623-017-0759-3

Katoh, Y. (2014). A simulation study of the propagation of whistler-mode chorus in the Earth's inner magnetosphere. *Earth, Planets and Space*, *66*, 6. https://doi.org/10.1186/1880-5981-66-6

Katoh, Y., & Omura, Y. (2004). Acceleration of relativistic electrons due to resonant scattering by whistler mode waves generated by temperature anisotropy in the inner magnetosphere. *Journal of Geophysical Research*, *109*, A12214. https://doi.org/10.1029/2004JA010654

Katoh, Y., & Omura, Y. (2006). A study of generation mechanism of VLF triggered emission by self-consistent particle code. *Journal of Geophysical Research*, *111*, A12207. https://doi.org/10.1029/2006JA011704

Katoh, Y., & Omura, Y. (2007). Computer simulation of chorus wave generation in the Earth's inner magnetosphere. *Geophysical Research Letters*, *34*, L03102. https://doi.org/10.1029/2006GL028594

Katoh, Y., & Omura, Y. (2011). Amplitude dependence of frequency sweep rates of whistler mode chorus emissions. *Journal of Geophysical Research*, *116*, A07201. https://doi.org/10.1029/2011JA016496

Katoh, Y., & Omura, Y. (2013). Effect of the background magnetic field inhomogeneity on generation processes of whistler-mode chorus and broadband hiss-like emissions. *Journal of Geophysical Research: Space Physics*, *118*, 4189–4198. https://doi.org/10.1002/jgra.50395

Katoh, Y., & Omura, Y. (2016). Electron hybrid code simulation of whistler-mode chorus generation with real parameters in the Earth's inner magnetosphere. *Earth, Planets and Space*, *68*, 192. https://doi.org/10.1186/s40623-016-0568-0

Katoh, Y., Ono, T., & Iizima, M. (2005). Numerical simulation of resonant scattering of energetic electrons in the outer radiation belt. *Earth, Planets and Space*, *57*(2), 117–124. https://doi.org/10.1186/BF03352555

Katoh, Y., Omura, Y., Miyake, Y., Nakashima, H., Usui, H., & Fukazawa, K. (2016). *Electron hybrid code simulations with OhHelp load balancer for the study of relativistic electron acceleration in planetary magnetospheres*. Paper presented at 35th Japan Society for Simulation Technology Annual Conference, Kyoto, Japan.

Katoh, Y., Kojima, H., Hikishima, M., Takashima, T., Asamura, K., Miyoshi, Y., … Shinohara, I. (2018). Software-type wave-particle interaction analyzer on board the Arase satellite. *Earth, Planets and Space*, *70*. https://doi.org/10.1186/s40623-017-0771-7

Kazama, Y., Wang, B.-J., Wang, S.-Y., Ho, P. T. P., Tam, S. W. Y., Chang, T. F., … Asamura, K. (2017). Low-energy electron instrument onboard the Arase satellite. *Earth, Planets and Space*, *69*, 165. https://doi.org/10.1186/s40623-017-0748-6

Kennel, C. F., & Petschek, H. E. (1966). Limit on stable trapped particle fluxes. *Journal of Geophysical Research*, *71*, 1–28.

Kurita, S., Katoh, Y., Omura, Y., Angelopoulos, V., Cully, C. M., Le Contel, O., & Misawa, H. (2012). THEMIS observation of chorus elements without a gap at half the gyrofrequency. *Journal of Geophysical Research*, *117*, A11223. https://doi.org/10.1029/2012JA018076

Li, W., Bortnik, J., Thorne, R. M., & Angelopoulos, V. (2011). Global distribution of wave amplitudes and wave normal angles of chorus waves using THEMIS wave observations. *Journal of Geophysical Research*, *116*, A12205. https://doi.org/10.1029/2011JA017035

Li, W., Thorne, R. M., Bortnik, J., Tao, X., & Angelopoulos, V. (2012). Characteristics of hiss-like and discrete whistler-mode emissions. *Geophysical Research Letters*, *39*, L18106. https://doi.org/10.1029/2012GL053206

Li, W., Santolik, O., Bortnik, J., Thorne, R. M., Kletzing, C. A., Kurth, W. S., & Hospodarsky, G. B. (2016). New chorus wave properties near the equator from Van Allen Probes wave observations. *Geophysical Research Letters*, *43*, 4725–4735. https://doi.org/10.1002/2016GL068780

Macúšová, E., Santolík, O., Cornilleau-Wehrlin, N., & Yearby, K. H. (2015). Bandwidths and amplitudes of chorus-like banded emissions measured by the TC-1 Double Star spacecraft. *Journal of Geophysical Research: Space Physics*, *120*, 1057–1071. https://doi.org/10.1002/2014JA020440

Miyoshi, Y., Ono, T., Takashima, T., Asamura, K., Hirahara, M., Kasaba, Y., … Segawa, T. T. (2012). The energization and radiation in geospace (ERG) project. In D. Summers, et al. (Eds.), *Dynamics of the Earth's radiation belts and inner magnetosphere*, *Geophysical Monograph Series* (Vol. 199, pp. 243–254). Washington, DC:: American Geophysical Union. https://doi.org/10.1029/2012GM001304

Miyoshi, Y., Saito, S., Seki, K., Nishiyama, T., Kataoka, R., Asamura, K., … Santolik, O. (2015). Relation between fine structure of energy spectra for pulsating aurora electrons and frequency spectra of whistler mode chorus waves. *Journal of Geophysical Research: Space Physics*, *120*, 7728–7736. https://doi.org/10.1002/2015JA021562

Nakashima, H., Miyake, Y., Usui, H., & Omura, Y. (2009). OhHelp: A scalable domain-decomposing dynamic load balancing for particle-in-cell simulations. In *Proceedings of the 23rd international conference on Supercomputing* (pp. 90-99).

Nunn, D., & Rycroft, M. J. (2005). A parametric study of triggered VLF emissions and the control of radio emission frequency sweep rate. *Annales de Geophysique*, *23*, 1–12.

Nunn, D., Rycroft, M., & Trakhtengerts, V. (2005). A parametric study of the numerical simulations of triggered VLF emissions. *Annales de Geophysique*, *23*(12), 3655–3666. https://doi.org/10.5194/angeo-23-3655-2005

Omura, Y., & Nunn, D. (2011). Triggering process of whistler mode chorus emissions in the magnetosphere. *Journal of Geophysical Research*, *116*, A05205. https://doi.org/10.1029/2010JA016280

Omura, Y., Katoh, Y., & Summers, D. (2008). Theory and simulation of the generation of whistler-mode chorus. *Journal of Geophysical Research*, *113*, A04223. https://doi.org/10.1029/2007JA012622

Omura, Y., Hikishima, M., Katoh, Y., Summers, D., & Yagitani, S. (2009). Nonlinear mechanisms of lower-band and upper-band VLF chorus emissions in the magnetosphere. *Journal of Geophysical Research*, *114*, A07217. https://doi.org/10.1029/2009JA014206

Ozaki, M., Yagitani, S., Sawai, K., Shiokawa, K., Miyoshi, Y., Kataoka, R., … Jordanova, V. K. (2015). A direct link between chorus emissions and pulsating aurora on timescales from milliseconds to minutes: A case study at subauroral latitudes. *Journal of Geophysical Research: Space Physics*, *120*, 9617–9631. https://doi.org/10.1002/2015JA021381

Santolík, O., Gurnett, D. A., Pickett, J. S., Parrot, M., & Cornilleau-Wehrlin, N. (2003). Spatio-temporal structure of storm-time chorus. *Journal of Geophysical Research*, *108*(A7), 1278. https://doi.org/10.1029/2002JA009791

Santolík, O., Kletzing, C. A., Kurth, W. S., Hospodarsky, G. B., & Bounds, S. R. (2014). Fine structure of large-amplitude chorus wave packets. *Geophysical Research Letters*, *41*, 293–299. https://doi.org/10.1002/2013GL058889

Summers, D., Tang, R., & Thorne, R. M. (2009). Limit on stably trapped particle fluxes in planetary magnetospheres. *Journal of Geophysical Research*, *114*, A10210. https://doi.org/10.1029/2009JA014428

Summers, D., Tang, R., & Omura, Y. (2011). Effects of nonlinear wave growth on extreme radiation belt electron fluxes. *Journal of Geophysical Research*, *116*, A10226. https://doi.org/10.1029/2011JA016602

Tang, R., Summers, D., & Deng, X. (2014). Effects of cold electron number density variation on whistler-mode wave growth. *Annales de Geophysique*, *32*(7), 889–898. https://doi.org/10.5194/angeo-32-889-2014

Thorne, R. M., Ni, B., Tao, X., Horne, R. B., & Meredith, N. P. (2010). Scattering by chorus waves as the dominant cause of diffuse auroral precipitation. *Nature*, *467*(7318), 943–946. https://doi.org/10.1038/nature09467

Tsurutani, B. T., & Smith, E. J. (1974). Postmidnight chorus: A substorm phenomenon. *Journal of Geophysical Research*, *79*(1), 118–127. https://doi.org/10.1029/JA079i001p00118

Turner, D. L., Angelopoulos, V., Li, W., Bortnik, J., Ni, B., Ma, Q., … Rodriguez, J. V. (2014). Competing source and loss mechanisms due to wave-particle interactions in Earth's outer radiation belt during the 30 September to 3 October 2012 geomagnetic storm. *Journal of Geophysical Research: Space Physics*, *119*, 1960–1979. https://doi.org/10.1002/2014JA019770

Turner, D. L., O'Brien, T. P., Fennell, J. F., Claudepierre, S. G., Blake, J. B., Kilpua, E. K. J., & Hietala, H. (2015). The effects of geomagnetic storms on electrons in Earth's radiation belts. *Geophysical Research Letters*, *42*, 9176–9184. https://doi.org/10.1002/2015GL064747

Wang, C.-P., Lyons, L. R., Angelopoulos, V., Larson, D., McFadden, J. P., Frey, S., … Magnes, W. (2008). THEMIS observations of penetration of the plasma sheet into the ring current region during a magnetic storm. *Geophysical Research Letters*, *35*, L17S14. https://doi.org/10.1029/2008GL033375

Xiao, F., Thorne, R. M., & Summers, D. (1998). Instability of electromagnetic R-mode waves in a relativistic plasma. *Physics of Plasmas*, *5*(7), 2489–2497. https://doi.org/10.1063/1.872932

Yagitani, S., Habagishi, T., & Omura, Y. (2014). Geotail observation of upper band and lower band chorus elements in the outer magnetosphere. *Journal of Geophysical Research: Space Physics*, *119*, 4694–4705. https://doi.org/10.1002/2013JA019678